IEEE Access
Multidisciplinary | Rapid Review | Open Access Journal

Received February 8, 2021, accepted March 11, 2021, date of publication March 18, 2021, date of current version March 30, 2021.

Digital Object Identifier 10.1109/ACCESS.2021.3066970

Distributed ADMM Using Private Blockchain for Power Flow Optimization in Distribution Network With Coupled and Mixed-Integer Constraints

CHINMAY SHAH[1], (Student Member, IEEE), JENNIFER KING[2], (Member, IEEE), AND RICHARD W. WIES[1], (Senior Member, IEEE)

[1]Department of Electrical and Computer Engineering, The University of Alaska Fairbanks, Fairbanks, AK 99709, USA
[2]National Renewable Energy Laboratory, Golden, CO 80401, USA

Corresponding author: Chinmay Shah (cshah@alaska.edu)

This work was supported in part by the U.S. Department of Energy through the Battelle Memorial Institute under Contract DEAC05-76RL01830, in part by the subcontract from Pacific Northwest National Laboratories to the University of Alaska Fairbanks under Contract 474633, in part by the National Renewable Energy Laboratory, operated by Alliance for Sustainable Energy, LLC, for the U.S. Department of Energy (DOE) under Contract DE-AC36-08GO28308, in part by the U.S. Department of Energy Office of Energy Efficiency and Renewable Energy and the Wind Energy Technologies Office, and in part by the U.S. Department of Energy Office of Science, Office of Basic Energy Sciences, EPSCoR Program; Office of Electricity Microgrid R&D Program; and Office of Energy Efficiency and Renewable Energy Solar Energy Technology Office under Grant DE-SC0020281. The support for article processing charge was provided by the University of Alaska Fairbanks Office of Vice Chancellor for Research.

ABSTRACT The optimization problem for scheduling distributed energy resources (DERs) and battery energy storage systems (BESS) integrated with the power grid is important to minimize energy consumption from conventional sources in response to demand. Conventionally this optimization problem is solved in a centralized manner, limiting the size of the problem that can be solved and creating a high communication overhead because all the data is transferred to the central controller. These limitations are addressed by the proposed distributed consensus-based alternating direction method of multiplier (DC-ADMM) optimization algorithm, which decomposes the optimization problem into subproblems with private cost function and constraints. The distribution feeder is partitioned into low coupling subnetworks/regions, which solves the private subproblem locally and exchanges information with the neighboring regions to reach consensus. The relaxation strategy is employed for mixed-integer and coupled constraints introduced in the optimal power flow (OPF) problem by stationary and transportable BESS because DC-ADMM convergence is only guaranteed for strict convex problems. The information exchange and synchronization between subnetworks/regions are vital for distributed optimization. In this work, both of these aspects are addressed by the blockchain. The smart contract deployed on the blockchain network acts as a mediator for secure data exchange and synchronization in distributed computation. The blockchain-based distributed optimization problem's effectiveness is tested for a 0.5-MW laboratory microgrid for one hour ahead and day-ahead for the IEEE 123-bus and EPRI J1 test feeders, and results are compared with a centralized solution.

INDEX TERMS Alternating direction method of multiplier, battery energy storage systems, blockchain, distributed optimization, optimal power flow, microgrid.

I. INTRODUCTION

Power distribution networks are being reshaped by the integration of distributed energy resources (DERs) and battery energy storage systems (BESS) [1]. These DERs, when used intelligently, can reduce our dependence on conventional energy resources and thereby decrease the generation cost to meet the demand [2]. The optimal power flow (OPF)–economic dispatch problem [3] seeks to optimize the objective of minimizing the total generation cost while satisfying the constraints imposed by the distribution network and device operating limits.

The OPF problem is challenging to solve because of the nonconvex feasible set and, hence, convex relaxation would ease the computation complexity [4]. The second-order cone program (SOCP) relaxation for the power distribution network is proposed in [5]–[9]. The SOCP relaxed OPF problem can be solved using any convex optimization solver. The authors of [10]–[12] have proposed algorithms for optimal power flow in power distribution networks with integrated

The associate editor coordinating the review of this manuscript and approving it for publication was Dipankar Deb.

BESS which are solved centrally. A centralized approach to solve the OPF problem in power distribution networks with a large number of integrated DERs and BESS is computationally challenging and exhibits poor scalability. A distributed optimization algorithm can address this challenge.

Several distributed optimization algorithms have been adapted and/or developed in recent years to solve the OPF problem, which decomposes the central problem into local subproblems. The algorithm in [13] is based on a dual decomposition method and in [14], [15] on the auxiliary variable method. The alternating direction method of multiplier (ADMM) [16], which is simultaneously general and scalable, is exploited in most of the recent research work to solve the OPF problem in a distributed fashion. The ADMM algorithm in [17], [18] solves the OPF problem, exchanging voltage information between the neighboring regions; however, DERs and BESS are not integrated into the test network. A full-scale distributed OPF is implemented using ADMM in [4], [19]–[23] in which participating nodes/controllers exchange information with the system or virtual aggregator to solve for the global update. The OPF problem with nonconvex feasible sets in [24]–[28] is solved using a decentralized algorithm in which a specific node communicates only with its adjacent nodes with no central or virtual aggregator. The authors in [26] discuss about the computation time and convergence of the algorithm and have not addressed the impacts and uncertainties of DER and energy storage integration, which is resolved in [27]. The algorithm proposed in [28] exchanges voltage and phase angle information with the neighboring microgrids to reach consensus and does not consider the impact of energy storage integration or consensus on active and reactive power flow between the interconnected microgrids.

In all the published work mentioned above, the microgrids or the distribution network partitions are considered static. In this work, the power distribution network is partitioned dynamically based on our previous work presented in [29]. The OPF problem for the distribution network partitioned into subnetworks is separable in which each subnetwork has a private cost function and private constraints. The need for a central/virtual aggregator to solve the separable distributed OPF problem is eliminated by implementing a distributed consensus based alternating direction method of multipliers (DC-ADMM) proposed in [30]–[32]. The DC-ADMM converges only for strictly convex problems. The mutually exclusive charging and discharging status of BESS introduces mixed-integer constraints to the OPF problem. The relax-and-fix (RF) heuristic algorithm discussed in [33]–[36] is employed for mixed-integer constraints that can be handled by DC-ADMM. The issue of DER and load curtailment is tackled by transportable BESS. The constraints for transportable BESS are coupled, which are decomposed, relaxed, and augmented into the objective function. The optimal route scheduling and connection stations for transportable BESS are already discussed in [37] and [38] respectively and not in the scope of this work. The blockchain-based technology

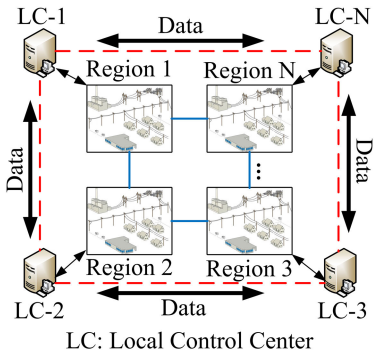

FIGURE 1. Schematic of data exchange between local controllers to solve distributed optimization.

is employed for direct and reliable exchange of information between the participating nodes or assets by establishing a secure and tamper-proof digital platform [39], [40]. The blockchain has been used in [22] to store the optimal schedule and to make automatic and secure payments.

The information exchange between the neighboring regions/nodes is essential to solve the distributed optimization problem as shown in Fig. 1. As discussed in [41], there are two kinds of communications infrastructure for information exchange: 1) centralized infrastructure and 2) distributed infrastructure. The supervisory control and data acquisition (SCADA) system is an example of centralized infrastructure, where local devices or remote terminal units (RTUs) send the data to the central controller and cannot exchange information among each other. The limitation of centralized infrastructure is that the fault in the central controller can halt the entire network. With the recent developments in internet of things (IoT) technology, the local controllers and RTUs can communicate with each other [42] and are an example of distributed communication infrastructure.

The main objective of this research is to implement an offline DC-ADMM OPF problem on a blockchain platform. The main contributions of this research work are as follows:

1) Presenting a day ahead dispatch strategy for a dynamically partitioned power distribution network using a DC-ADMM OPF algorithm.
2) A DC-ADMM and RF heuristic algorithm to solve the OPF problem with mixed-integer and coupled BESS constraints is proposed.
3) The proposed DC-ADMM-based OPF algorithm utilizes the blockchain network and smart contract to broadcast information to the neighboring subnetworks, enable synchronization between the local controllers of the subnetworks, and schedule transportable BESS to curb DER and load curtailment. The system/virtual aggregator or the global update is not needed in the proposed approach. Advanced distribution management systems could deploy smart contracts in existing utility grids.
4) The proposed DC-ADMM-based OPF algorithm is tested for the Alaska Center for Energy and Power (ACEP) 0.5-MW Power System Integration (PSI)

Laboratory Microgrid [59] and IEEE 123-bus and EPRI J1 test feeders for scalability.

The rest of the paper is organized as follows: Section II describes the formulation of the OPF problem, BESS model, blockchain, and smart contract. The DC-ADMM and RF heuristic algorithm implemented on the blockchain network are explained in Section III, followed by the test feeder network formulation in Section IV. The simulation results are presented in Section V. Section VI concludes the paper and discusses future work, followed by acknowledgments.

II. PROBLEM FORMULATION

In this section, we define an OPF problem for the power distribution network. The distribution network includes a substation node, renewable energy resources, customer-owned BESS, ISO-owned BESS, mobile BESS, fixed loads, and electric vehicles (EVs) as shapeable loads.

A. DISTRIBUTION NETWORK MODEL

The radial graph distributed network model $\Re := (\mathcal{N}, \varepsilon)$ where $\mathcal{N} := \{0, 1, 2 \ldots, n\}$ represents the set of nodes, and ε represents the set of distribution lines connecting these nodes in the network. $\mathcal{N} = 0$ represents the root node, and the other nodes in $\mathcal{N}$ represent the branch nodes. For each node i, it has a unique parent node A_i and a set of children nodes $C_i = [j_i, j_2, \ldots, j_k]$ [4]. For each line that connects node i to its parent node A_i, let $z_i = r_i + jx_i$ be the impedance of the line.

For each node $i \in \mathcal{N}$, let V_i be the complex voltage, $v_i = |V_i|^2$, and $s_i = p_i + jq_i$ be the net complex power injection. Let I_i be the complex current flowing from node i to parent node A_i, $l_i = |I_i|^2$, and $S_i = P_i + jQ_i$ be the complex power flowing from node i to child node C_i. The branch flow model for this radial network is given by:

$$p_i(t) = P_i(t) - \sum_{k \in C_i} P_k(t) + r_i l_i(t), \quad \forall i \in \mathcal{N} \tag{1a}$$

$$q_i(t) = Q_i(t) - \sum_{k \in C_i} Q_k(t) + x_i l_i(t), \quad \forall i \in \mathcal{N} \tag{1b}$$

$$v_i(t) = V_{A_i}(t) + 2(r_i P_i(t) + x_i Q_i(t)) - (r_i^2 + x_i^2) l_i(t) \tag{1c}$$

$$|S_i(t)|^2 = v_i(t) l_i(t), \quad \forall i \in \mathcal{N} \tag{1d}$$

where $t = 1, 2, 3, \ldots, T$, and $T = 24\ h$.

B. NETWORK CONSTRAINTS

The set of network components at a particular node i for time t is denoted as:
$p_i^g(t)$ - Dispatchable synchronous generators (DSG) / substation active power
$p_i^{pv}(t)$ - Photovoltaic (PV) generator unit active power
$p_i^{wind}(t)$ - Wind turbine active power
$p_i^{cob-ch}(t)$ - customer-owned BESS (charging) active power
$p_i^{cob-dch}(t)$ - customer-owned BESS (discharging) active power
$p_i^{ISOb-ch}(t)$ - ISO-owned BESS (charging) active power
$p_i^{ISOb-dch}(t)$ - ISO-owned BESS (discharging) active power
$p^{tb-ch}(t)$ - Transportable BESS (charging) active power
$p^{tb-dch}(t)$ - Transportable BESS (discharging) active power
$p_i^{fl}(t)$ - Fixed load
$p_i^{evl}(t)$ - Electric Vehicle (EV) load
$q_i^g(t)$ - Diesel generator/substation reactive power
$q_i^{fl}(t)$ - Fixed load (reactive)
$\underline{p_i}, \overline{p_i}$ - Minimum and maximum power generation or consumption respectively.

The net active and reactive power injection at a particular node i is given by:

$$\begin{aligned} p_i(t) = {} & p_i^g(t) + p_i^{pv}(t) + p_i^{wind}(t) + p_i^{cob-dch}(t) \\ & + p_i^{ISOb-dch}(t) - p_i^{cob-ch}(t) - p_i^{ISOb-ch}(t) \\ & - p_i^{fl}(t) - p_i^{evl}(t) \end{aligned} \tag{2a}$$

$$q_i(t) = q_i^g(t) - q_i^{fl}(t) \tag{2b}$$

1) DISPATCHABLE SYNCHRONOUS GENERATOR (DSG)

The practical constraints for the DSG, including spinning reserve and prohibited operating zones, are defined in this subsection [43]. The power output and ramp rate constraints are:

$$\underline{p_i^g} \le p_i^g(t) \le \overline{p_i^g} \tag{3a}$$

$$p_i^g(t-1) - DR_i \le p_i^g(t) \le p_i^g(t-1) + UR_i, \forall i \tag{3b}$$

where $\underline{p_i^g}$ and $\overline{p_i^g}$ are the minimum and maximum generation limits of DSG at bus i, respectively, and DR_i and UR_I are down-ramp-rate and up-ramp-rate limits of all online DSG units, respectively. The spinning reserve constraints for DSG units on $(\mathcal{N} - \omega)$ buses are:

$$p_{S_R}(t) \ge \eta_{S_R} p_i^{fl}(t) \tag{3c}$$

$$\sum_{i \in (\mathcal{N})} p_{S_i}(t) \ge p_{S_R}(t) \tag{3d}$$

$$p_{S_i}(t) \le \overline{p_i^g} - p_i^g, \forall i \in (\mathcal{N}) \tag{3e}$$

$$p_{S_i}(t) \le \overline{p_{S_i}}, \forall i \in (\mathcal{N}) \tag{3f}$$

where $p_{S_R}(t)$ is the distribution network spinning reserve requirement, η_{S_R} is the required percentage of spinning reserve, p_{S_i} is the spinning reserve contribution of the DSG unit on bus i, and $\overline{p_{S_i}}$ is the maximum spinning reserve contribution of the DSG unit on bus i.

2) CUSTOMER-OWNED BESS

The customer-owned BESS model considered in this research work is based on the dispatch strategy that maximizes battery utilization. The mixed-integer linear BESS model, which is dependent on charge and discharge cycle efficiencies and ignores losses as well as the degradation defined in [44], has the following constraints:

$$p_i^{cob}(t) = \eta_{ch} p_i^{cob-ch}(t) - \frac{1}{\eta_{dch}} p_i^{cob-dch}(t) \tag{4a}$$

$$\underline{E_i^{cob}} \le E_{i0}^{cob} + \Delta t \sum_{\tau=1}^{T-1} p_i^{cob(k)} \le \overline{E_i^{cob}} \tag{4b}$$

$$0 \le p_i^{cob-ch}(t) \le \chi_i^{cob-ch}(t)\overline{p_i^{cob-ch}} \tag{4c}$$

$$0 \le p_i^{cob-dch}(t) \le \chi_i^{cob-dch}(t)\overline{p_i^{cob-dch}} \tag{4d}$$

$$\chi_i^{cob-ch}(t) + \chi_i^{cob-dch}(t) \le 1 \tag{4e}$$

where $\chi_i^{cob-ch}(t)$, $\chi_i^{cob-dch}(t) \in \{0, 1\}$ is mutually exclusive, $i \in \mathcal{N}$, $t = 0, 1, 2, \ldots, T-1$, and $T = 24\ h$. $\underline{E_i^{cob}}$ and $\overline{E_i^{cob}}$ are the minimum and maximum capacities of the BESS.

3) ISO-OWNED BESS

The ISO-integrated BESS is a viable and cost-effective solution to account for the variability and uncertainty of loads and renewable energy resources in the power distribution network. But the degradation and ohmic power losses in BESS are inevitable. The BESS model incorporating ohmic power losses is defined as,

$$p_i^{ISOb-loss}(t)v_i(t) \ge r_i^{eq}(p_i^{ISOb}(t))^2 + r_i^{cvt}(q_i^{ISOb}(t))^2 \tag{5a}$$

$$r_i^{eq}(\overline{s_i^{cvt}})^2 \ge p_i^{ISOb-loss}(t)\underline{v_i} + r_i^{ISOb}(q_i^{ISOb}(t))^2 \tag{5b}$$

$$(\overline{s_i^{cvt}})^2(\underline{v_i} + \overline{v_i}) \ge \overline{s_i^{cvt}}^2 v_i(t) + p_i^{ISOb-loss}(t)(\underline{v_i} * \overline{v_i}) \tag{5c}$$

$$(p_i^{ISOb}(t))^2 + (q_i^{ISOb}(t))^2 \le (\overline{s_i^{cvt}})^2 \tag{5d}$$

$$p_i^{ISOb}(t) = \eta_{ch}p_i^{ISOb-ch}(t) - \frac{1}{\eta_{dch}}p_i^{ISOb-dch}(t) + p_i^{ISOb-loss}(t) \tag{5e}$$

$$\underline{E_i^{ISOb}} \le E_{i0}^{ISOb} + \Delta t \sum_{\tau=1}^{T-1} p_i^{ISOb(k)} \le \overline{E_i^{ISOb}} \tag{5f}$$

$$0 \le p_i^{ISOb-ch}(t) \le \chi_i^{ISOb-ch}(t)\overline{p_i^{ISOb-ch}} \tag{5g}$$

$$0 \le p_i^{ISOb-dch}(t) \le \chi_i^{ISOb-dch}(t)\overline{p_i^{ISOb-dch}} \tag{5h}$$

$$\chi_i^{ISOb-ch}(t) + \chi_i^{ISOb-dch}(t) \le 1 \tag{5i}$$

where $\chi_i^{ISOb-ch}(t)$, $\chi_i^{ISOb-dch}(t) \in \{0, 1\}$ is mutually exclusive, $i \in \mathcal{N}$, $t = 0, 1, 2, \ldots, T-1$, and $T = 24\ h$. $\underline{E_i^{ISOb}}$ and $\overline{E_i^{ISOb}}$ are minimum and maximum capacities of the BESS. $p_i^{ISOb-loss}(t)$ is the ohmic power loss of the BESS, $r_i^{eq} = r_i^b + r_i^{cvt}$ is the sum of battery energy storage and associated converter resistance and, $\overline{s_i^{cvt}}$ is the maximum apparent output power of the converter. The degradation cost function of BESS in [45] is incorporated into the optimal power flow objective function and is given by:

$$f_i(p_i^{ISOb}(t)) = c_d * max\left(\begin{bmatrix} a_1 & a_2 & a_3 \end{bmatrix}\begin{bmatrix} p_i^{ISOb}(t) \\ E_i^{ISOb}(t) \\ \overline{E_i^{ISOb}} \end{bmatrix}\right) \tag{6}$$

where $a_1, a_2, a_3 \in \mathcal{R}^{n_p X 1}$ are plane parameters of n_p triangles from the convex hull, $E_i^{ISOb}(t)$ is the state of energy of ISO-owned BESS at time t, and c_d is the degradation cost of the BESS whose optimal value is tabulated in [46].

4) WIND POWER GENERATION

The operational constraint for wind power is given by,

$$0 \le p_i^{wind}(t) \le \overline{p_i^{wind}}(t) \tag{7}$$

where $p_i^{wind}(t)$ is the actual utilization of the wind power and $\overline{p_i^{wind}}(t)$ is the available wind power at time t based on the forecast.

5) PV POWER GENERATION

The operational constraint for the PV power generating unit is given by,

$$0 \le p_i^{pv}(t) \le \overline{p_i^{pv}}(t) \tag{8}$$

where $p_i^{PV}(t)$ is the actual utilization of the wind power and $\overline{p_i^{PV}}(t)$ is the available wind power at time t based on the forecast.

6) TRANSPORTABLE BESS

The transportable BESS can be used as a nonspinning reserve, and its sizing is based on the criteria defined in [47] and [48]. The transportable BESS is also scheduled to minimize the curtailment of renewable energy resources and load shedding. The mixed-integer linear model of transportable BESS is considered in this research with the following operation and scheduling constraints.

$$\sum_{i=0}^{\mathcal{N}}(\overline{p_i^{pv}(t)} + \overline{p_i^{wind}(t)} - p_i^{cob-ch}(t) - p_i^{ISOb-ch}(t) - p_i^{fl}(t) - p_i^{evl}(t)) \le p_i^{tb-ch}(t) \tag{9a}$$

$$\sum_{i=0}^{\mathcal{N}}(p_i^{fl}(t) + p_i^{evl}(t) - p_i^{g}(t) - p_i^{pv}(t) - p_i^{wind}(t) - p_i^{cob-dch}(t) - p_i^{ISOb-dch}(t)) \le p^{tb-dch}(t) \tag{9b}$$

$$\underline{E^{tb}} \le E_0^{tb} + \Delta t \sum_{\tau=1}^{T-1} \eta_{ch}p^{tb-ch}(t) - \frac{1}{\eta_{dch}}p^{tb-dch}(t) \le \overline{E^{tb}} \tag{9c}$$

$$0 \le p_i^{tb-ch}(t) \le \chi_i^{tb-ch}(t)\overline{p_i^{tb-ch}} \tag{9d}$$

$$0 \le p_i^{tb-dch}(t) \le \chi_i^{tb-dch}(t)\overline{p_i^{tb-dch}} \tag{9e}$$

$$\chi_i^{tb-ch}(t) + \chi_i^{tb-dch}(t) \le 1 \tag{9f}$$

$\chi_i^{tb-ch}(t)$, $\chi_i^{tb-dch}(t) \in \{0, 1\}$ is mutually exclusive, $i \in \mathcal{N}$, $t = 0, 1, 2, \ldots, T-1$, and $T = 24\ h$. $\underline{E_i^{tb}}$ and $\overline{E_i^{tb}}$ are minimum and maximum capacities of the BESS.

7) ELECTRIC VEHICLE LOAD

The EVs with the energy demand E_i^{evl} have the following constraints,

$$\underline{p_i^{evl}} \le p_i^{evl}(t) \le \overline{p_i^{evl}} \tag{10a}$$

$$\sum_{t}^{T=24h} p_i^{evl}(t) = E_i^{evl} \tag{10b}$$

$$p_i^{evl}(t) = 0 \forall t = 1, 2, \ldots, t_{i,start} \quad (10c)$$
$$p_i^{evl}(t) = 0 \forall t = t_{i,stop}, \ldots, T \quad (10d)$$

where the electric vehicle must be charged between $t_{i,start}$ and $t_{i,stop}$. The EV batteries are only considered as load while charging and are not considered for grid operations in this research work because of degradation and reduction in their life cycle.

8) CENTRALIZED OPF AND SOCP RELAXATION OF NETWORK CONSTRAINTS

The thermal generator cost at the substation node is typically represented by a quadratic fuel cost function given by:

$$f_i(p_i^g(t)) = \alpha_i(p_i^g(t))^2 + \beta_i p_i^g(t) + \gamma_i(t) \quad (11)$$

where α, β, γ are the fuel cost parameter.

The OPF problem aims at minimizing the thermal generation and battery degradation cost subject to branch flow equations and local DER constraints and is formulated as,

$$min \sum_{t=1}^{T} \sum_{i=0}^{\mathcal{N}} f_i(p_i^g(t)) + f_i(p_i^{IOSb}(t)) \quad (12a)$$
$$s.t.\ (1a) - (1d),\ (2a) - (2b),\ (3a) - (3f),\ (4a) - (4e)$$
$$(5a) - (5i),\ (7),\ (8),\ (9a) - (9f),\ (10a) - (10d) \quad (12b)$$

The quadratic equality constraint in (1d) makes the above OPF problem nonconvex. The OPF problem can be relaxed to a convex problem by SOCP relaxation of (1d) given by,

$$|S_i(t)|^2 \leq v_i(t) l_i(t), \quad \forall i = 0, 1, 2, \ldots, \mathcal{N} \quad (13)$$

The binary variables in constraints (4c)-(4d) and (5g)-(5h) make OPF a mixed-integer problem and its relaxation is explained in the next section.

C. BLOCKCHAIN AND SMART CONTRACT

Blockchain is a prominent technology that provides a secure and distributed database that contains the log of transactions in chronological order. The digital users/nodes on this blockchain network communicate through the peer-to-peer (P2P) system to reach a consensus on the ledger's valid state. This is contrary to centralized systems, which need the central authority to act as the intermediary to maintain the database and transactions and guard its authenticity. Furthermore, the blockchain network's security is enhanced by hash functions and public-key cryptography and depends on the type of network (i.e., public or private network) [49]. Users can either join the public blockchain network or the private blockchain network. The trust among the users emerges from game-theoretical incentives in the public network with the permissionless ledger. The public network provides a tamperproof and censorship-resistant system. On the contrary, the private network with the permissioned ledger has reduced security but is fast, easy to scale, and energy-efficient [50].

The full potential of blockchain technology can only be utilized using smart contracts. The smart contract is a user-defined executable program that can alter the ledger and perform specific tasks when called upon by the users. The Ethereum is an open-source programmable distributed computing platform with smart contract functionality [51]. The distributed OPF algorithm proposed in this paper is developed on the private Ethereum network in which the smart contract is deployed to act as a mediator for secure communication between the local controllers and a scheduler. The workflow showing the interaction between the smart contract, local microgrid controllers, and distribution network components while solving the distributed OPF problem is explained in this work. The following two subsections explain in brief how blockchain can be implemented on IoT networks or traditional SCADA systems.

D. BLOCKCHAIN AND INTERNET OF ENERGY (IoE)

The integration of distributed energy resources and energy storage has made the power distribution network decentralized and bidirectional. Hence, the distribution network requires a distributed communication architecture where network components can exchange electricity among themselves so that the distribution is effective, autonomous, and without the central authority's involvement. This bidirectional and distributed communication can be achieved by the Internet of Energy (IoE). The IoE coordinates various network components with the help of the internet. However, the IoE technology faces many privacy and security issues that can be overcome by blockchain [52], [53].

E. BLOCKCHAIN AND SCADA

SCADA systems are an integral part of the power distribution network for automatic generation control and economic dispatch [54], [55]. A SCADA system comprises a centralized control center and associated field devices, local control modules, and RTUs. The central control center solves the optimization problem and dispatches the control signal to the network's field devices. As a result, the power distribution network with the existing conventional SCADA makes the entire network vulnerable to cyberattacks and control center faults. The blockchain-based end-to-end secure prototype for SCADA with smart RTUs linked with each other and the central control center by IoT cloud services is developed in [55], [56] for practical implementation.

III. DISTRIBUTED OPF PROBLEM FORMULATION

In this section, the distributed optimization algorithm based on consensus ADMM is presented to solve the OPF problem. First, the power distribution network is partitioned into several subnetworks/regions. After that, the general form DC-ADMM is described and then applied to solve the OPF problem. Once the solution method is established, the algorithm is implemented on the blockchain network.

A. POWER DISTRIBUTION NETWORK PARTITION

The power distribution network is initially partitioned by unnormalized spectral clustering analysis. Once the initial partitions are formed, the power distribution network is

re-partitioned by the algorithm described in our previous work [29]. After the optimal partitions are achieved, the OPF problem is decomposed as explained in the next subsection.

B. DISTRIBUTED CONSENSUS-BASED ADMM (DC-ADMM)

A unidirected network denoted by $\Re := (\mathcal{N}, \varepsilon)$, where $\mathcal{N} := \{0, 1, 2 \ldots, n\}$ represents the set of nodes, and ε represents the set of edges connecting these nodes. The node i and j can communicate information only if $(i, j) \in \varepsilon$ (i.e., node j is the neighbor to node i). Each node $i \in \mathcal{N}$ has a local objective function which is given by

$$\min_{x} \sum_{i=0}^{\mathcal{N}} f_i(x_i) \tag{14a}$$

$$s.t.\ Ax = 0 \tag{14b}$$

where $x_i \in \mathcal{R}^{\mathcal{N}}$ is a local variable that is related to the local problem, and $Ax = 0$ implies that $x_i = x_j$ for nodes i and j connected by an edge (i, j).

The augmented Lagrangian function for the problem in (14) is given by

$$\mathcal{L}(x, u) = \sum_{i=0}^{\mathcal{N}} f_i(x_i) + u_i^T(x_i) + \frac{\rho}{2}||Ax_i||_2^2 \tag{15}$$

where the dual variable $u_i^T \in \mathcal{R}^{\mathcal{N}}$, and $\rho > 0$ is the penalty parameter. The iterations to solve the general form consensus ADMM problem mentioned in (15) is given by

$$x_i^{k+1} = \underset{x_i}{argmin} f_i(x_i) + \frac{\rho_1}{2} \sum_{j \in A_i} ||x_j^{k+1} - x_i - \frac{1}{\rho_1} u_{ji}^k||_2^2 + \frac{\rho_2}{2} \sum_{j \in C_i} ||x_i - x_j^k - \frac{1}{\rho_2} u_{ij}^k||_2^2 \tag{16a}$$

$$u_{ji}^{k+1} = u_{ji}^k - \rho_1 (x_j^{k+1} - x_i^{k+1}) \ \ \forall j \in A_i \tag{16b}$$

$$u_{ij}^{k+1} = u_{ij}^k - \rho_2 (x_i^{k+1} - x_j^k) \ \ \forall j \in C_i \tag{16c}$$

where ρ_1 and ρ_2 are penalty parameters, u_{ij} is the dual variable with the constraints $x_i = x_j$ on the edge $(i, j) \in \varepsilon$. Each node i keeps a local copy of decision variable $x_i \in \mathcal{R}^{\mathcal{N}}$ and a vector of a dual variable u_{ji} with $j \in A_i$. The algorithm will stop when the following condition is met:

$$\Delta x_i^{k+1} = |x_i^{k+1} - x_i^k| \leq \epsilon_{tol} \tag{17}$$

where ϵ_{tol} is the tolerance value of the residual.

C. DC-ADMM MODIFICATION FOR MIXED-INTEGER PROBLEMS

The optimization problems with integer or binary variables are nonconvex, and the convergence of those problems when solved using ADMM is not guaranteed. The mixed-integer problem (MIP) in this work is solved by the RF heuristic algorithm.

The local subproblem for node i defined in (16) is an MIP for $x_z \in \{0, 1\} \subset x_i$. Initially to solve the MIP using RF, all the binary variables are relaxed (i.e., they can take any value between 0 and 1) defined as $0 \leq x_z \leq 1$. This makes the problem in (16) a convex quadratic problem for which the ADMM converges. Once the initial solution is obtained, a few variables are enforced to be binary variables, with the remaining ones relaxed. After finding the solution, the binary variables are fixed and another set of relaxed variables are enforced to be a binary variable. The process iterates until all the binary variables are fixed and a feasible solution is obtained. Once all the binary variables are fixed, the ADMM will converge because all the subproblems are convex.

D. APPLICATION OF DC-ADMM AND RF TO OPF

To solve the distributed OPF problem, the distribution network is partitioned into several subnetworks/regions, as explained in III-A. Now the OPF problem for the entire distribution network is reformulated to solve using the DC-ADMM based method so that each region needs to solve its local subproblem in each iteration. The local subproblem has its own objective function and set of constraints and is formulated for a particular region i as

$$\min \sum_{t=1}^{T} \sum_{i=0}^{\mathcal{N}} f_i(p_i^g(t)) + f_i(p_i^{IOSb}(t)) \tag{18a}$$

$$s.t.\ (1a) - (1d),\ (2a) - (2b),\ (3a) - (3f),\ (4a) - (4e)\ (5a) - (5i),\ (7),\ (8),\ (9a) - (9f),\ (10a) - (10d),\ (13) \tag{18b}$$

The local variables to solve the subproblem presented in (18b) for a particular region i is denoted by $x_i = [p_i, q_i, p_i^g, q_i^g, p_i^{pv}, p_i^{wind}, p_i^{cob-ch}, p_i^{cob-dch}, p_i^{ISOb-ch}, p_i^{ISOb-dch}, p_i^{fl}, q_i^{fl}, p_i^{evl}]$ and is not shared over the network. All the variables and constraints defined above are local except the constraints (1a)-(1c), (9a), and (9b). The equation in (9a) and (9b) is decomposed for a particular region i as

$$\overline{p_i^{pv}(t)} + \overline{p_i^{wind}(t)} - p_i^{cob-ch}(t) - p_i^{ISOb-ch}(t) - p_i^{fl}(t) - p_i^{evl}(t)) \leq p_i^{tb-ch}(t) \tag{19a}$$

$$p_i^{fl}(t) + p_i^{evl}(t) - p_i^g(t) - p_i^{pv}(t) - p_i^{wind}(t) - p_i^{cob-dch}(t) - p_i^{ISOb-dch}(t) \leq p_i^{tb-dch}(t) \tag{19b}$$

where $p_i^{tb-ch}(t)$ and $p_i^{tb-dch}(t)$ are the local representation of the global variables $p^{tb-ch}(t)$ and $p^{tb-dch}(t)$, respectively, for a region i. The constraints (1a)-(1c), (19a), and (19b) are augmented in the objective function of the problem in (18b) and solved iteratively as

$$x_i^{k+1} = \underset{x_i}{argmin} \sum_{t=1}^{T} f_i(p_i^g(t)) + f_i(p_i^{IOSb}(t)) + + \frac{\rho_1}{2} \sum_{j \in A_i} ||v_j^{k+1} - v_i - \frac{1}{\rho_1} u_{ji}^k||_2^2 + \frac{\rho_2}{2} \sum_{j \in C_i} ||x_i - x_j^k - \frac{1}{\rho_2} u_{ij}^k||_2^2 \tag{20a}$$

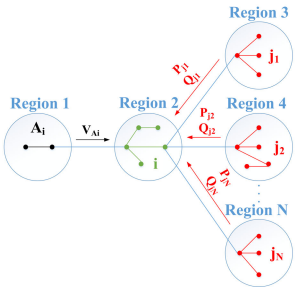

FIGURE 2. Information exchange between neighboring subnetworks/regions in power distribution network.

$$u_{ji}^{k+1} = u_{ji}^{k} - \rho_1(v_j^{k+1} - v_i^{k+1}) \ \forall j \in A_i \tag{20b}$$
$$u_{ij}^{k+1} = u_{ij}^{k} - \rho_2(x_i^{k+1} - x_j^{k}) \ \forall j \in C_i \tag{20c}$$

The local coupling variable $x_j = [v_j, p_j^{tb-ch}, p_j^{tb-dch}]$, $\forall j \in A_i$ and $x_j = [\sum_{j\in C_i} P_j, \sum_{j\in C_i} Q_j, \sum_{j\in C_i} p_j^{tb-ch}, \sum_{j\in C_i} p_j^{tb-dch}]$, $\forall j \in C_i$ will be shared with the neighboring subnetworks/regions as shown in Fig. 2.

The subproblem for region i defined in (20c) contains four binary variables χ_i^{cob-ch}, $\chi_i^{ISOb-ch}$, $\chi_i^{cob-dch}$, *and* $\chi_i^{ISOb-dch}$ for charging and discharging status, respectively, of the customer-owned and ISO-owned BESS. Initially, all four variables are relaxed and allowed to take any value between 0 and 1. This converts the subproblems in the convex quadratic problem and is solved until the acceptable tolerance of ϵ is achieved. After that, the variables for charging mode χ_i^{cob-ch}, $\chi_i^{ISOb-ch}$ are enforced to be the binary variables, and the OPF problem is solved until the tolerance ϵ is achieved or reaches the iteration limit. If the algorithm reaches the iteration limit with no feasible binary solution, the values of ρ_1 and ρ_2 are updated by 5% and warm start the OPF subproblem. In the last step, all the binary variables are fixed based on the condition in (21b), and the OPF problem is solved until it converges. The algorithm flowchart is shown in Fig. 3.

$$\chi_i^{cob-ch}(t) + \chi_i^{cob-dch}(t) \le 1 \tag{21a}$$
$$\chi_i^{ISOb-ch}(t) + \chi_i^{ISOb-dch}(t) \le 1 \tag{21b}$$

E. IMPLEMENTING THE ALGORITHM ON BLOCKCHAIN NETWORK

The private Ethereum blockchain network is used to implement the distributed OPF algorithm for the distribution network in this research work, and the block diagram is shown in Fig. 4. The go-ethereum client (geth) is used to run a full Ethereum node. Each node/user on the Ethereum network is assigned a personal account defined by a private and public key. Their address indexes these accounts Π derived from the public key. There are two types of Ethereum accounts: 1) externally owned accounts (EOAs) and 2) contracts accounts. The EOA is controlled by a private key and can transfer ether or trigger a contract code. The contract account has its own code and is controlled by that code. The

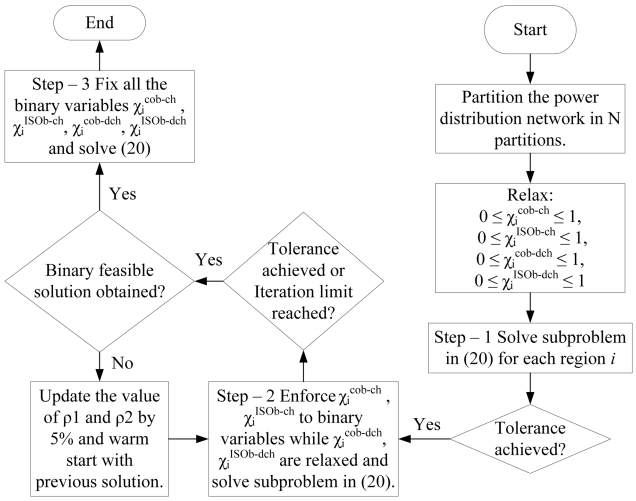

FIGURE 3. DC-ADMM and RF algorithm flowchart.

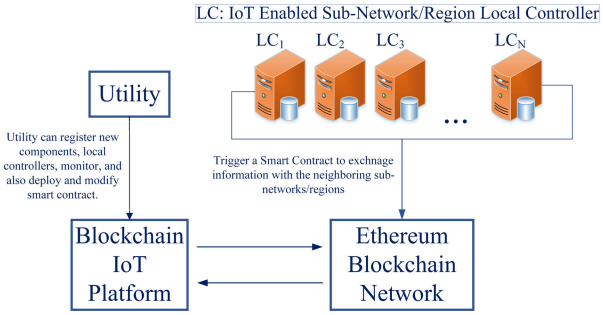

FIGURE 4. Ethereum blockchain network architecture for distributed OPF.

users/nodes interact with the Ethereum network by sending a transaction from an account using a web3 object that connects to a JSON-RPC server [57].

Upon establishing the Ethereum network to implement the DC-ADMM + RF for the OPF problem, an externally owned account indexed by address Π_i is set up for every region i in the distribution network. The contracts account indexed by address Ψ is set up for the control center that deploys the smart contract (modeled in Solidity [58]) to the network. The address Ψ is shared with all subnetwork/regions i in the network to communicate with the smart contract.

IV. CASE STUDY

In this section, we discuss validating the centralized and proposed DC-ADMM + RF OPF algorithms using results from a 0.5-MW laboratory microgrid at the ACEP PSI laboratory with four control nodes and implementing the same for the IEEE 123-bus and EPRI J1 test feeder system.

A. ACEP PSI LABORATORY MICROGRID

The ACEP PSI lab operates on the same scale as one of Alaska's village power systems and can be modified for individual test scenarios. The PSI lab infrastructure

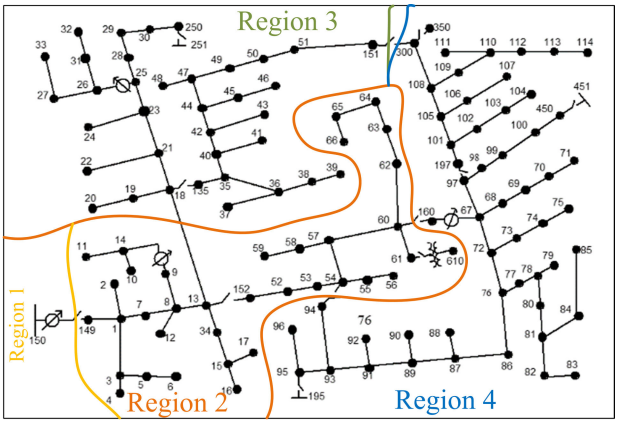

FIGURE 5. IEEE 123-bus test feeder partitioned into 4 subnetworks/regions for distributed OPF.

includes a 320-kW diesel generator, a 100-kW wind emulator, a 540-VDC/1000 A-hr lead-acid battery, a 312-kVA inverter, and two 250-kW programmable load banks. The one-line diagram of the ACEP PSI lab is available in [59].

B. IEEE 123-BUS TEST NETWORK

The IEEE 123-bus test feeder used in this study consists of 114 branch buses and is partitioned into four regions, as shown in Fig. 5. The test feeder is also modified to a balanced network [60]. The nominal operating voltage of the test feeder is 4.16 kV. The DC-ADMM + RF optimization algorithm in (20c) and Fig. 3 is implemented for the partitioned IEEE 123-bus test feeder, where each region solves its local subproblem and exchanges information with the neighboring regions.

Region 1 is a root/reference bus, either a substation or thermal/diesel generator with a quadratic fuel cost function. Other regions consist of branch nodes with a deterministic load profile, rooftop PV, wind farm, electric vehicle load, customer-owned BESS, ISO-owned BESS, and transportable BESS. The shapeable loads and customer-owned BESS at each node are half the peak residential load. The storage capacity of customer-owned BESS is 6 hours. The ISO-owned BESS has a peak power of 150-kW with a storage capacity of 4 hours. The ISO-owned BESS are considered on bus 39 and 85. The transportable BESS has a peak power rating of 1,000-kW with a storage capacity of 2 hours.

The PECAN STREET project residential load data set from January 1 to June 30, 2017, is used in this research work [61]. The capacity of the rooftop PV installed at each house on branch nodes is 6-kW. The hourly 2017 NSRDB solar data [62] from January 1 to June 30, 2017, is used for the rooftop PV. The wind farm is integrated with the network at bus 85. The wind farm consists of 6 wind turbines rated at 235-kW, each with a pole height of 35 m. The hourly NREL Flatirons Campus data for a wind turbine from January 1 to January 30, 2017, is used for this work [63].

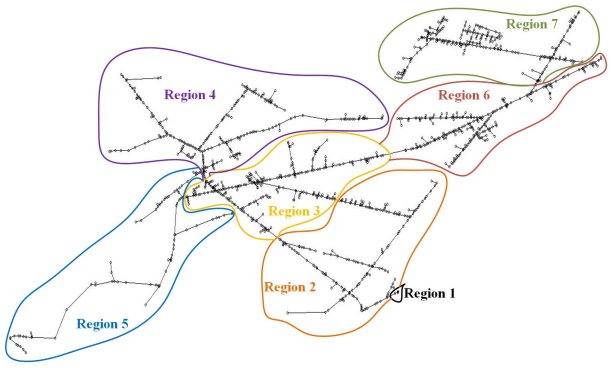

FIGURE 6. EPRI J1 test feeder partitioned into 7 subnetworks/regions for distributed OPF.

C. EPRI J1 FEEDER

The EPRI J1 test feeder has 3,434 buses, which serves approximately 1,300 residential, commercial, and light industrial customers via 58 miles of 12.47 kV primary line [64]. The feeder is modified to a balanced three phase network and is partitioned into seven regions as shown in Fig. 6 for this work. Region 1 is a substation, whereas other regions consist of branch nodes with residential, commercial, and light industrial load, residential rooftop PV, customer-owned large PV system, wind farms, electric vehicle loads, customer-owned BESS, ISO-owned BESS, and transportable BESS. The peak load of the entire feeder is approximately 6 MW. The shapeable load at each node with residential load is half the peak load. The 1.7-MW customer-owned PV system already exists on the feeder. Additionally, rooftop PV and customer-owned BESS rated 50% of each residential load's daily consumption are also considered in this research work. The storage capacity of customer-owned BESS is 6 hours. The hourly June 2012 solar data from EPRI [64] is used for PV. Two wind farms are integrated with the network, each consisting of 9 wind turbines. Each wind turbine is rated at 235-kW with a pole height of 35 m as in the IEEE 123-bus test feeder system. The hourly NREL Flatirons Campus data for a wind turbine from June 1 to June 30, 2012, is used for this work [63]. Four ISO-owned BESS rated with peak power 1,000-kW and storage capacity of 2 hours is also integrated with the network. The transportable BESS has a peak power rating of 1,000-kW with a storage capacity of 2 hours.

D. IMPLEMENTING THE TEST SYSTEM ON ETHEREUM NETWORK

The go-ethereum/Geth client is installed for running the ethereum node on the computer and is used to connect to the private ethereum network. Upon setting up the network, the smart contract to securely exchange the data with the neighboring regions for the DC-ADMM + RF OPF problem for the ACEP PSI lab, IEEE 123-bus, and EPRI J1 test feeder is developed and compiled in Solidity. The local subproblems are executed using Python and CVXPY. After solving the local subproblems, each region in the ACEP PSI lab, IEEE

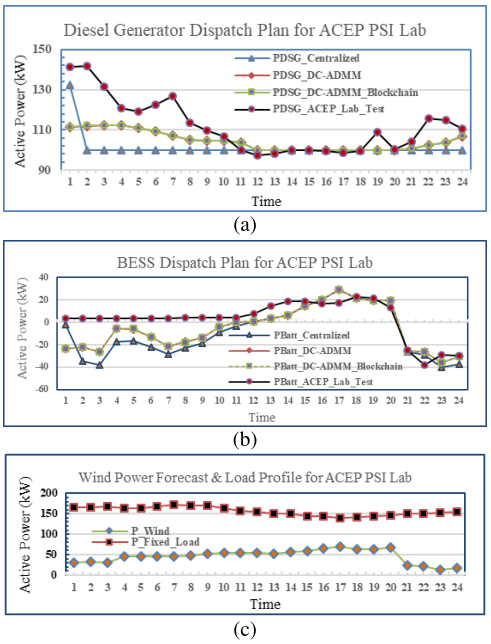

FIGURE 7. (a) ACEP PSI lab Diesel Generator Dispatch Plan, (b) ACEP PSI lab BESS Dispatch Plan, (c) ACEP PSI lab wind and load profile.

TABLE 1. Electric energy generation/consumption over 1 h for ACEP PSI lab.

OPF Type	Diesel Gen (kWh)	BESS Charge (kWh)	BESS Discharge (kWh)	Wind Gen (kWh)	Fixed Load (kWh)
Centralized	101.356	5.517	14.482	46.183	156.5
DC-ADMM + RF	104.435	5.517	11.399	46.183	156.5
DC-ADMM + RF - Blockchain	104.435	5.517	11.399	46.183	156.5
ACEP PSI Lab Test Results	111.707	6.237	5.093	53.742	162.33

123-bus, and EPRI J1 test feeder communicates with the Ethereum network using web3.py.

V. RESULTS

A. ACEP PSI LAB

An hour-ahead centralized OPF algorithm was tested in the 0.5-MW ACEP PSI laboratory. The lab's real-time control strategy is based on spinning reserve control (SRC). The SRC maintains the loading on the diesel-electric generator between the minimum and maximum set points using the inverter to compensate for over or under loading conditions. The OPF algorithms were simulated for 1 hour with a time step of 2.5 minutes. The dispatch plan for the diesel generator and BESS and wind and load profile used for testing is shown in Fig. 7. The constraints for BESS to simulate the OPF problem for ACEP PSI lab are based on ISO-owned BESS defined in (5a) to (5i).

The comparison of centralized and DC-ADMM + RF OPF dispatch plan for the ACEP PSI lab model with the lab test results is presented in Table 1 and Table 2.

We can observe from Fig. 7, Table 1, and Table 2 the minimum generation from the diesel electric generator is 100 kW which was set to prevent wet stacking in the diesel engine. The BESS discharges to the net load and charges from the excessive wind power. Also, there is a vast difference in the energy discharge from BESS between the OPF algorithms dispatch plan and lab test results. This difference is because, for the first half, the lab test was intentionally performed without employing any optimization strategy and only the diesel electric generator fed the loads while BESS remained idle. The dispatch plan generated for diesel generators and BESS is similar for DC-ADMM + RF with and without blockchain. The Table 2 also shows the difference in wind energy forecast and actual generation.

TABLE 2. Comparison of OPF algorithm dispatch plan with ACEP PSI lab test results.

Gen. Type	Centralized OPF-Lab Test Results (% Difference)	DC-ADMM OPF+RF-Lab Test Results (% Difference)	DC-ADMM+RF OPF with Blockchain-Lab Test Results (% Difference)
Diesel Generator	9.72 %	6.73 %	6.73 %
BESS Charging	12.25 %	12.25 %	12.25 %
BESS Discharging	95.93 %	76.47 %	76.47 %
Wind Generation	15.13 %	15.13 %	15.13 %
Fixed Load	3.65 %	3.65 %	3.65 %

TABLE 3. Comparison of DC-ADMM + RF OPF algorithm dispatch plan with centralized solution for IEEE 123-bus test feeder.

Gen. Type	Centralized OPF-DC-ADMM+RF OPF (% Difference)	Centralized OPF-DC-ADMM+RF OPF with Blockchain (% Difference)	DC-ADMM+RF OPF - DC-ADMM+RF OPF with Blockchain (% Difference)
DSG/Fuel Generator	9.34 %	7.188 %	1.3269 %
COB Charging	1.67487 %	0.7495 %	0.9322 %
COB Discharging	4.3636 %	2.4382 %	1.9735 %
ISOB Charging	1.5455 %	1.1854 %	0.3644 %
ISOB Discharging	2.7619 %	0.6631 %	2.1128 %

B. IEEE 123-BUS AND EPRI J1 TEST FEEDER

The centralized algorithm was tested using the IEEE 123-bus test feeder and the results are published in [44]. The comparison between the dispatch plan for the IEEE 123-bus test feeder generated using the centralized algorithm and DC-ADMM + RF with and without blockchain network is shown in Fig. 8 and Table 3.

We can observe from the results in Fig. 8 and Table 3 for IEEE 123-bus test feeder that the dispatch plan generated by DC-ADMM + RF with and without the communication over the blockchain network coincides with each other. The dispatch plan generated by the centralized algorithm is offset from the distributed algorithm, but the net generation/consumption over the 24-hour period is approximately similar. Hence, it is safe to assume that the proposed DC-ADMM + RF's performance quality is comparable to the standard centralized OPF algorithm.

Fig. 8(c) shows that the customer-owned BESS responds to the demand and charges from the excessive solar and wind power generation. The ISO-owned BESS remains idle during certain hours and only responds when necessary to reduce the charge-discharge cycle and minimize the degradation cost. From Fig. 8(a), we can observe that there is a sudden rise in the wind power generation at hour 5, which charges the customer-owned and ISO-owned BESS. As a result, there is not enough energy storage available during the peak solar hours. The transportable BESS is scheduled to charge from

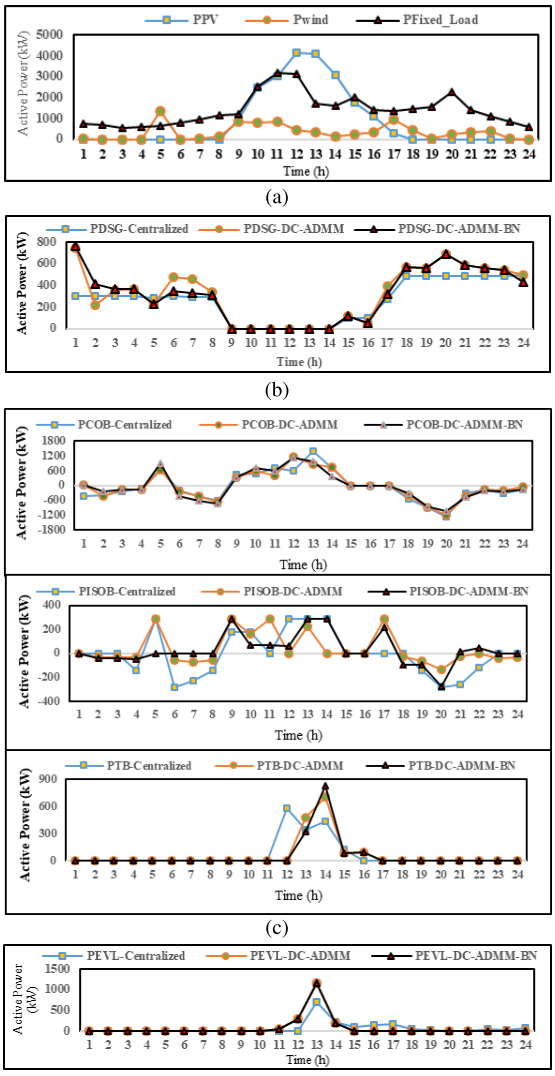

FIGURE 8. IEEE 123-bus test feeder (a) Residential PV, wind farm, and residential load profile, (b) distributed synchronous/fuel generator dispatch, (c) customer-owned BESS (COB), independent system operator BESS (ISOB), transportable BESS (TB) dispatch, and (d) Electric vehicle load scheduling generated by centralized, DC-ADMM + RF algorithm with and without blockchain.

excessive solar and wind generation, which reduces its curtailment. Also, the electric vehicles' charging schedule is generated for the peak solar and wind power generation hours.

The charge and discharge cycles for BESS are mutually exclusive, which makes the OPF problem mixed-integer. The proposed DC-ADMM + RF method in this paper solves the mixed-integer OPF problem, and the mutually exclusive charge and discharge cycles of the customer-owned and ISO-owned BESS for IEEE 123-bus test system are shown in Fig. 9. The negative values of active power represent the discharge cycle.

The algorithms are also tested for the EPRI J1 test feeder, and similar results were obtained. The comparison between the DC-ADMM + RF and centralized OPF results for the EPRI J1 test feeder is shown in Table 4.

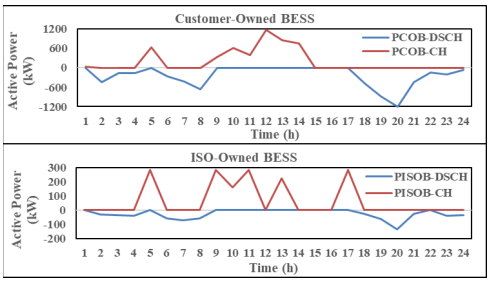

FIGURE 9. Mutually exclusive charge and discharge cycles for customer-owned and ISO-owned BESS.

TABLE 4. Comparison of DC-ADMM OPF algorithm dispatch plan with centralized solution for EPRI J1 test feeder.

Gen. Type	Centralized OPF-DC-ADMM+RF OPF (% Difference)	Centralized OPF-DC-ADMM+RF OPF with Blockchain (% Difference)	DC-ADMM OPF-DC-ADMM OPF with Blockchain (% Difference)
DSG/Fuel Generator	0.55 %	0.4832 %	1.0361 %
COB Charging	3.0212 %	0.3532 %	3.363 %
COB Discharging	1.1182 %	1.3366 %	2.44 %
ISOB Charging	5.595 %	5.535 %	0.062 %
ISOB Discharging	6.266 %	5.6113 %	0.6942 %

C. COMPUTATION DETAILS

For the ACEP PSI lab, IEEE 123-bus, and EPRI J1 test feeder, the centralized OPF problem is simulated in a Python-based, open-source optimization modeling language, Pyomo, and the proposed distributed optimization algorithm is simulated using CVXPY.

The simulations are run on a Windows 10 PC with a 3.40-GHz Intel Core i7 processor and 16-GB RAM. The solver used and computation time for each OPF algorithm simulation are listed in Table 5. For the DC-ADMM + RF OPF, the subproblem for each region is computed sequentially. As seen from Table 5, the computation time to solve the DC-ADMM + RF OPF problem is reduced compared to the centralized one for the IEEE 123-bus and the EPRI J1 test feeder. Hence, the algorithm is scalable and will be able to handle much larger systems where centralized OPF will be computationally intensive.

For the DC-ADMM + RF on a blockchain network, the time taken to validate the transactions is approximately 125 seconds for the ACEP PSI lab model, 625.2 seconds for the IEEE 123-bus, and 1,560 seconds for the EPRI J1 test system. The validation time is significantly high because each node transacts with the network sequentially. In practice on edge computing devices, these transactions would be performed in parallel, providing speed up by the factor equivalent to the number of regions the power distribution network is partitioned and will be demonstrated in future work by setting up a node1 for each region on the blockchain network using Docker.

The penalty parameters ρ_1 and ρ_2 were initialized to a value of 3. The penalty parameters are updated by 5% if no feasible binary solution is obtained. The iteration limit to obtain the feasible binary solution to fix the binary variables is set to 30 and tolerance value $\epsilon_{tol} = 1e-4$. The convergence results of DC-ADMM + RF for the IEEE 123-bus and the

TABLE 5. OPF algorithm computation time and solver.

		OPF Type		
		Centralized	DC-ADMM + RF	DC-ADMM + RF -Blockchain
Solver		Gurobi	Gurobi	Gurobi
Initial Computation Time for Step-1 DC-ADMM (seconds)	ACEP PSI Lab	-	0.0035	0.0035
	IEEE 123-bus Test Feeder	-	0.22	0.22
	EPRI J1 Test Feeder	-	0.38	0.38
Number of Iterations for Step-1 DC-ADMM	ACEP PSI Lab	-	24	24
	IEEE 123-Bus Test Feeder	-	67	67
	EPRI J1 Feeder	-	99	99
Number of Iterations for Step-3 DC-ADMM+RF	ACEP PSI Lab	-	5	6
	IEEE 123-Bus Test Feeder	-	18	18
	EPRI J1 Feeder	-	30	30
Total Computation Time for OPF (seconds)	ACEP PSI Lab	0.01199	1.9	1.9
	IEEE 123-Bus Test Feeder	27.4	20.2	20.2
	EPRI J1 Feeder	135.7	45.2	45.2

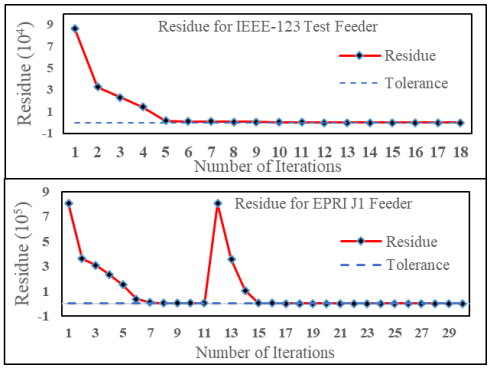

FIGURE 10. Residue for IEEE 123-bus and EPRI J1 test feeder.

EPRI J1 test feeder are shown in Fig. 10. We can observe that the DC-ADMM OPF converges in 18 and 30 iterations for the IEEE 123-bus and the EPRI J1 test feeder, respectively, after the binary variables are fixed.

The algorithm is part of a resiliency application for fault-tolerant energy system (RAFTES), which is being developed to integrate with the open-source ADMS platform GridAPPS-D [65]. The GridAPPS-D will act as a contracts account and deploy and manage the smart contract on the private Ethereum network. The algorithm will subscribe to the GridAPPS-D topic to receive the forecast data for the DERs integrated with the power grid. A practical demonstration on the GridAPPS-D platform will be presented in future work.

VI. CONCLUSION

A DC-ADMM + RF algorithm was proposed for the OPF problem with mixed-integer and coupled constraints for an adaptive partitioned power distribution network. The proposed algorithm successfully fixes the mixed-integer/binary variable, and the DC-ADMM converges for the OPF problem. We demonstrate that the proposed algorithm results are comparable by testing it for the 0.5-MW ACEP PSI laboratory microgrid. We can also conclude that the results obtained for the IEEE 123-bus and EPRI J1 test feeder for the proposed algorithm are similar to the standard centralized algorithm and hence scalable. The computation time of DC-ADMM + RF is also reduced compared to the centralized OPF, and hence it can be concluded that the algorithm converged faster with reliable results. When implemented on the blockchain network, the proposed algorithm takes more time to validate the nodes, but it provides secure communication and synchronization between the subnetwork local controllers.

The proposed distributed algorithm in this research work is offline; therefore, its solution is applied to the physical grid only after it converges. In the future, we need to explore ways to reduce the computation time for distributed algorithms implemented on the blockchain network to be applied to real-time/online optimization and control.

ACKNOWLEDGMENT

The contributions to this research work were achieved in part through the Grid Modernization Laboratory Consortium (GMLC), a strategic partnership between the U.S. Department of Energy and the National Laboratories. The GMLC was established as part of the U.S. Department of Energy's Grid Modernization Initiative (GMI) to accelerate the modernization of the U.S. electricity infrastructure. This work was also authored [in part] by the National Renewable Energy Laboratory, operated by Alliance for Sustainable Energy, LLC, for the U.S. Department of Energy (DOE) under Contract No. DE-AC36-08GO28308. The views expressed in the article do not necessarily represent the views of the DOE or the U.S. Government. The U.S. Government retains and the publisher, by accepting the article for publication, acknowledges that the U.S. Government retains a nonexclusive, paid-up, irrevocable, worldwide license to publish or reproduce the published form of this work, or allow others to do so, for U.S. Government purposes.

The authors would like to thank Dr. Ron Melton, Dr. Kevin Schneider, and Dr. Thomas McDermott at Pacific Northwest National Laboratory (PNNL) for their support. They are also thankful to the Alaska Center for Energy and Power (ACEP) and the University of Alaska Fairbanks for providing the data and resources needed for this research work.

REFERENCES

[1] G. Rackliffe. (2019). *Distributed Grid Management 101: Ders Are Reshaping the Power Grid*. [Online]. Available: https://www.abb-conversations.com/2019/02/distributed-grid-management-101-ders-are-reshaping-the-power-grid/

[2] K. Cleary and K. Palmer. (2020). *Renewables 101: Integrating Renewable Energy Resources Into the Grid*. [Online]. Available: https://www.rff.org/publications/explainers/renewables-101-integrating-renewables/

[3] O. Alsac, J. Bright, M. Prais, and B. Stott, "Further developments in LP-based optimal power flow," *IEEE Trans. Power Syst.*, vol. 5, no. 3, pp. 697–711, Aug. 1990.

[4] Q. Peng and S. H. Low, "Distributed optimal power flow algorithm for radial networks," *IEEE Trans. Smart Grid*, vol. 9, no. 1, pp. 111–121, 2018.

[5] R. Jabr, "Radial distribution load flow using conic programming," *IEEE Trans. Power Syst.*, vol. 21, no. 3, pp. 1458–1469, Jul. 2006.

[6] M. Farivar and S. H. Low, "Branch flow model: Relaxations and convexification—Part I," *IEEE Trans. Power Syst.*, vol. 28, no. 3, pp. 2554–2563, Apr. 2013.

[7] S. H. Low, "Convex relaxation of optimal power flow, I: Formulations and relaxations," *IEEE Trans. Control Netw. Syst.*, vol. 1, no. 1, pp. 15–27, Mar. 2014.

[8] M. Farivar and S. H. Low, "Branch flow model: Relaxations and convexification—Part II," *IEEE Trans. Power Syst.*, vol. 28, no. 3, pp. 2564–2572, Apr. 2013.

[9] S. H. Low, "Convex relaxation of optimal power flow, II: Formulations and relaxations," *IEEE Trans. Control Netw. Syst.*, vol. 1, no. 2, pp. 177–189, Mar. 2014.

[10] A. Gabash and P. Li, "Active-reactive optimal power flow in distribution networks with embedded generation and battery storage," *IEEE Trans. Power Syst.*, vol. 27, no. 4, pp. 2026–2035, Nov. 2012.

[11] M. Nick, R. Cherkaoui, and M. Paolone, "Optimal allocation of dispersed energy storage systems in active distribution networks for energy balance and grid support," *IEEE Trans. Power Syst.*, vol. 29, no. 5, pp. 2300–2310, Sep. 2014.

[12] M. Sufyan, C. Tan, N. A. Rahim, S. R. S. Raihan, and M. A. Muhammad, "Dynamic economic dispatch of isolated microgrid with energy storage using MIQP," in *Proc. Int. Conf. Intell. Adv. Syst. (ICIAS)*, Kuala Lumpur, Malaysia, Aug. 2018, pp. 1–6.

[13] A. Lam, B. Zhang, and D. N. Tse, "Distributed algorithms for optimal power flow problem," in *Proc. IEEE Conf. Decis. Control*, Maui, HI, USA, Dec. 2012, pp. 430–437.

[14] N. Li, L. Chen, and S. H. Low, "Demand response in radial distribution networks: Distributed algorithm," in *Proc. Conf. Rec. 46th Asilomar Conf. Signals, Syst. Comput. (ASILOMAR)*, Pacific Grove, CA, USA, Nov. 2012, pp. 1549–1553.

[15] E. Devane and I. Lestas, "Stability and convergence of distributed algorithms for the OPF problem," in *Proc. 52nd IEEE Conf. Decis. Control*, Florence, Italy, Dec. 2013, pp. 2933–2938.

[16] S. Boyd, N. Parikh, E. Chu, B. Peleato, and J. Eckstein, "Distributed optimization and statistical learning via the alternating direction method of multipliers," *Found. Trends Mach. Learn.*, vol. 3, no. 1, pp. 1–122, 2010.

[17] E. Dall'Anese, H. Zhu, and G. B. Giannakis, "Distributed optimal power flow for smart microgrids," *IEEE Trans. Smart Grid*, vol. 4, no. 3, pp. 1464–1475, Sep. 2013.

[18] T. Erseghe, "Distributed optimal power flow using ADMM," *IEEE Trans. Power Syst.*, vol. 29, no. 5, pp. 2370–2380, Sep. 2014.

[19] P. Scott, D. Gordon, E. Franklin, L. Jones, and S. Thiebaux, "Network-aware coordination of residential distributed energy resources," *IEEE Trans. Smart Grid*, vol. 10, no. 6, pp. 6528–6537, Nov. 2019.

[20] W. Huang, W. Zheng, and D. J. Hill, "Distributionally robust optimal power flow in multi-microgrids with decomposition and guaranteed convergence," *IEEE Trans. Smart Grid*, vol. 12, no. 1, pp. 43–55, Jan. 2021.

[21] X. Lu, H. Yin, S. Xia, D. Zhang, M. Shahidehpour, X. Zhang, and T. Ding, "A real-time alternating direction method of multipliers algorithm for nonconvex optimal power flow problem," *IEEE Trans. Ind. Appl.*, vol. 57, no. 1, pp. 70–82, Jan. 2021.

[22] E. Munsing, J. Mather, and S. Moura, "Blockchains for decentralized optimization of energy resources in microgrid networks," in *Proc. IEEE Conf. Control Technol. Appl.*, Maui, HI, USA, Aug. 2017, pp. 2164–2171.

[23] T. AlSkais and G. van Leeuwen, "Decentralized optimal power flow in distribution networks using blockchain," in *Proc. Int. Conf. Smart Energy Syst. Technol. (SEST)*, Porto, Portugal, Sep. 2019, pp. 1–6.

[24] A. X. Sun, D. T. Pham, and S. Ghosh, "Fully decentralized AC optimal power flow algorithms," in *Proc. IEEE PES Gen. Meeting*, Vancouver, BC, Canada, Jul. 2013, pp. 1–5.

[25] S. Magnusson, P. C. Weeraddana, and C. Fischione, "A distributed approach for the optimal power-flow problem based on ADMM and sequential convex approximations," *IEEE Trans. Control Netw. Syst.*, vol. 2, no. 3, pp. 238–253, Sep. 2015.

[26] S. Mhanna, G. Verbic, and A. C. Chapman, "Adaptive ADMM for distributed AC optimal power flow," *IEEE Trans. Power Syst.*, vol. 34, no. 3, pp. 2025–2035, May 2019.

[27] X. Chang, Y. Xu, W. Gu, H. Sun, M.-Y. Chow, and Z. Yi, "Accelerated distributed hybrid stochastic/robust energy management of smart grids," *IEEE Trans. Ind. Informat.*, early access, Sep. 7, 2020, doi: 10.1109/TII.2020.3022412.

[28] F. Li, J. Qin, Y. Wan, and T. Yang, "Decentralized cooperative optimal power flow of multiple interconnected microgrids via negotiation," *IEEE Trans. Smart Grid*, vol. 11, no. 5, pp. 3827–3836, Sep. 2020.

[29] C. Shah and R. Wies, "Adaptive day-ahead prediction of resilient power distribution network partitions," in *Proc. IEEE Green Technol. Conf. (GreenTech)*, Denver, CO, USA, Apr. 2021.

[30] E. Wei and A. Ozdaglar, "Distributed alternating direction method of multipliers," in *Proc. IEEE 51st IEEE Conf. Decis. Control (CDC)*, Maui, HI, USA, Dec. 2012, pp. 5445–5450.

[31] J. F. C. Mota, J. M. F. Xavier, P. M. Q. Aguiar, and M. Puschel, "D-ADMM: A communication-efficient distributed algorithm for separable optimization," *IEEE Trans. Signal Process.*, vol. 61, no. 10, pp. 2718–2723, May 2013.

[32] L. Jian, Y. Zhao, J. Hu, and P. Li, "Distributed inexact consensus-based ADMM method for multi-agent unconstrained optimization problem," *IEEE Access*, vol. 7, pp. 79311–79319, Jun. 2019.

[33] D. Ferreira, R. Morabito, and S. Rangel, "Relax and fix heuristics to solve one-stage one-machine lot-scheduling models for small-scale soft drink plants," *Comput. Oper. Res.*, vol. 37, no. 4, pp. 684–691, Apr. 2010.

[34] N. Brahimi, "A relax-and-fix heuristic for a production planning problem with order acceptance and flexible due dates," in *Proc. Int. Conf. Ind. Eng. Oper. Manage.*, Bali, Indonesia, Jan. 2014, pp. 7–9.

[35] C. F. M. Toledo, M. da Silva Arantes, M. Y. B. Hossomi, P. M. França, and K. Akartunalı, "A relax-and-fix with fix-and-optimize heuristic applied to multi-level lot-sizing problems," *J. Heuristics*, vol. 21, no. 5, pp. 687–717, Oct. 2015.

[36] F. Mohammadjavad, "Large-scale unit commitment: Decentralized mixed integer programming approaches," Ph.D. dissertation, Atlanta, GA, USA, Georgia Inst. Technol., Dec. 2015.

[37] S.-Y. Kwon, J.-Y. Park, and Y.-J. Kim, "Optimal V2G and route scheduling of mobile energy storage devices using a linear transit model to reduce electricity and transportation energy losses," *IEEE Trans. Ind. Appl.*, vol. 56, no. 1, pp. 34–47, Jan. 2020.

[38] H. H. Abdeltawab and Y. A.-R.-I. Mohamed, "Mobile energy storage scheduling and operation in active distribution systems," *IEEE Trans. Ind. Electron.*, vol. 64, no. 9, pp. 6828–6840, Sep. 2017.

[39] J. Mattila, T. Seppala, C. Naucler, R. Stahl, M. Tikkanen, A. Badenlid, and J. Seppala, "Industrial blockchain platforms: An exercise in use case development in the energy industry," Res. Inst. Finnish Economy, Helsinki, Finland, Tech. Rep. 43, Oct. 2016.

[40] M. Mikell. (2018). *S.A.V.E. From IoT: Trust and Tracking From a New IoT Blockchain Service*. [Online]. Available: https://www.ibm.com/blogs/internet-of-things/iot-new-blockchain-service/

[41] J. Guo, G. Hug, and O. K. Tonguz, "A distributed approach for the optimal power-flow problem based on admm and sequential convex approximations," *IEEE Trans. Ind. Informat.*, vol. 14, no. 7, pp. 2903–2913, Jul. 2018.

[42] IoT.nxt. (2018). *IoT and SCADA: Is One Going to Replace the Other?* [Online]. Available: https://iiot-world.com/industrial-iot/connected-industry/internet-of-things-and-scada-is-one-going-to-replace-the-other/

[43] L. G. Papageorgiou and E. S. Fraga, "A mixed integer quadratic programming formulation for the economic dispatch of generators with prohibited operating zones," *Electr. Power Syst. Res.*, vol. 77, no. 10, pp. 1292–1296, Aug. 2007.

[44] C. Shah and R. Wies, "Algorithms for optimal power flow in isolated distribution networks using different battery energy storage models," in *Proc. IEEE Power Energy Soc. Innov. Smart Grid Technol. Conf. (ISGT)*, Washington, DC, USA, Feb. 2020, pp. 1–5.

[45] P. Fortenbacher, J. Mathieu, and G. Andersson, "Modeling and optimal operation of distributed battery storage in low voltage grids," *IEEE Trans. Power Syst.*, vol. 32, no. 6, pp. 4340–4350, 2017.

[46] G. He, S. Kar, J. Mohammadi, P. Moutis, and J. Whitacre, "Power system dispatch with marginal degradation cost of battery storage," *IEEE Trans. Power Syst.*, early access, Dec. 31, 2021, doi: 10.1109/TPWRS.2020.3048401.

[47] NERC. *Operating Reserves*. Accessed: Jan. 20, 2021. [Online]. Available: https://www.nerc.com/files/BAL-STD-002-0.pdf

[48] California ISO. *Ancillary Services Market*. Accessed: Jan. 20, 2021. [Online]. Available: https://www.caiso.com/Documents/Chapter4.pdf

[49] M. Andoni, V. Robu, D. Flynn, S. Abram, D. Gleach, D. Jenkins, P. McCallum, and A. Peacock, "Blockchain technology in the energy sector: A systemetic review of challenges and opportunities," *Renew. Sustain. Energy Rev.*, vol. 100, pp. 143–174, Feb. 2019.

[50] J. Mattila, "The blockchain phenomenon: The disruptive potential of distributed consensus architectures," Res. Inst. Finnish Economy, Helsinki, Finland, Tech. Rep. 38, May 2016.

[51] (2020). *Ethereum*. [Online]. Available: https://ethereum.org/

[52] A. Miglani, N. Kumar, V. Chamola, and S. Zeadally, "Blockchain for Internet of energy management: Review, solutions, and challenges," *Comput. Commun.*, vol. 151, pp. 395–418, Feb. 2020.

[53] *IoT Powered by Blockchain*, Delloite, USA, 2018. [Online]. Available: https://www2.deloitte.com/content/dam/Deloitte/de/Documents/Innovation/IoT-powered-by-Blockchain-Deloitte.pdf
[54] Y. Xichang and Z. Quanren, "Practical implementation of the SCADA+AGC/ED system of the Hunan power pool in the central China power network," *IEEE Trans. Energy Convers.*, vol. 9, no. 2, pp. 250–255, Jun. 1994.
[55] A. Ullah, S. M. S. Siddiquee, M. A. Hossain, and S. K. Ray, "An ethereum blockchain-based prototype for data security of regulated electricity market," *Inventions*, vol. 5, no. 4, p. 58, Nov. 2020.
[56] M. T. Hossain, S. Badsha, and H. Shen, "PoRCH: A novel consensus mechanism for blockchain-enabled future SCADA systems in smart grids and industry 4.0," in *Proc. IEEE Int. IoT, Electron. Mechatronics Conf. (IEMTRONICS)*, Vancouver, BC, Canada, Sep. 2020, pp. 1–7.
[57] P. Merriam and J. Carver. (2018). *Web3py*. [Online]. Available: https://web3py.readthedocs.io/en/stable/overview.html
[58] (2016). *Solidity*. [Online]. Available: https://solidity.readthedocs.io/en/v0.6.8/index.html
[59] ACEP. *Power System Integration Laboratory*. Accessed: Jan. 15, 2021. [Online]. Available: http://acep.uaf.edu/media/174758/ACEP-PSI-2016-04-26-A-2-web.pdf
[60] B. B. Navarro, I. B. N. C. Cruz, and B. M. Malquisto, "Radial network reconfiguration and load balancing for loss minimization using genetic algorithms," in *Proc. TENCON IEEE Region Conf.*, Cebu, Philippines, Nov. 2012, pp. 1–6.
[61] *Pecanstreet Data*. Accessed: Jan. 1, 2020. [Online]. Available: https://dataport.pecanstreet.org/idq
[62] *Nsrdb*. Accessed: Jan. 31, 2021. [Online]. Available: https://nsrdb.nrel.gov/about/u-s-data.html
[63] D. Jager and A. Andreas, "NREL national wind technology center (NWTC): M2 tower," Boulder, CO, USA, Tech. Rep. DA-5500-56489. [Online]. Available: https://midcdmz.nrel.gov/apps/day.pl?NWTC, doi: 10.5439/1052222.
[64] *EPRI J1 Feeder, Distributed PV (DPV) Monitoring and Feeder Analysis*. Accessed: Sep. 8, 2020. [Online]. Available: https://dpv.epri.com/feeder_j.html
[65] *GridAPPS-D*. [Online]. Available: https://gridapps-d.org/

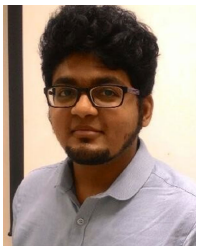

CHINMAY SHAH (Student Member, IEEE) received the B.Tech. degree in instrumentation and control engineering from Nirma University, India, in 2012, and the M.S. degree in electrical engineering from the University of Houston, TX, USA, in 2017. He is currently pursuing the Ph.D. degree in electrical engineering with the University of Alaska Fairbanks.

He worked as an Instrumentation and Control Engineer with Dodsal Engineering and Construction, Dubai, UAE, from 2012 to 2014. He also worked as a Research Intern with National Renewable Energy Laboratory, in Summer 2019. He is currently working as a Research Assistant with the Alaska Center for Energy and Power (ACEP). His research interests include modeling and control of power electronic converter-based DERs, distributed optimization, distributed controls for the power grid, power system resiliency and reliability, application of blockchain, and the Internet of Things (IoT) in the power distribution networks.

JENNIFER KING (Member, IEEE) received the B.S. degree in electrical engineering from the University of St. Thomas, St. Paul, MN, USA, in 2012, and the M.S. and Ph.D. degrees in aerospace engineering from the University of Minnesota, in 2014 and 2016, respectively.

She is currently a Senior Research Engineer with the National Renewable Energy Laboratory and working with the National Wind Technology Center, primarily on wind farm controls and optimization, autonomous energy systems, optimal design, and dispatch of hybrid energy systems. Her primary focus is on finding new ways to better integrate and operate renewable energy into the grid of the future. She leads a project on autonomous urbanization, where millions of vehicles, buildings, and other distributed energy resources are seamlessly integrated with the grid. Her current research interests include modeling and distributed control/optimization of large-scale hybrid systems.

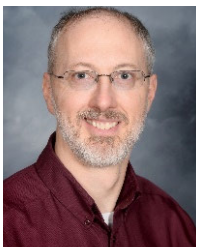

RICHARD W. WIES (Senior Member, IEEE) received the B.S., M.S., and Ph.D. degrees in electrical engineering from the University of Wyoming, Laramie, WY, USA, in 1992, 1995, and 1999, respectively.

Since 1999, he has been with The University of Alaska, Fairbanks, AK, USA, where he is currently a Professor with the Department of Electrical and Computer Engineering, with a concentration in electric power systems. He is also a licensed Professional Engineer with the State of Alaska. He leads research focused on the engineering challenges of renewable energy integration in remote islanded microgrids in collaboration with the Alaska Center for Energy and Power. He has served on the PES Power Systems Dynamic Performance and Power Engineering Education Committees, where he contributed to two task force reports. He has been invited to present a number of panels at IEEE sponsored conferences about his research work with remote islanded microgrids. His research interests include development of advanced distributed generation and load control schemes and optimal power dispatch strategies for remote islanded microgrids employing high penetrations of renewable energy, grid-forming operation with standalone asynchronous renewable generation, impacts of renewable power on food and water systems, and stability of converter-dominated grids.